

TS-PIELM: Time-Stepping Physics-Informed Extreme Learning Machine Facilities Soil Consolidation Analyses

Dr He Yang

E-mail: yanghesdu@mail.sdu.edu.cn

School of Qilu Transportation, Shandong University, Jinan, 250002, China

Dr Fei Ren

Email: ren87@outlook.com

Faculty of Mechanical Engineering, Qilu University of Technology (Shandong Academy of Sciences),
Jinan, 250353, China

Prof Hai-Sui Yu, FREng, DVC and Provost

E-mail: Yu.H@leeds.ac.uk

School of Civil Engineering, University of Leeds, Leeds, LS2 9JT, UK

Professor Xueyu Geng

Email: Xueyu.Geng@warwick.ac.uk

School of Engineering, University of Warwick, Coventry, CV4 7AL, UK

Professor Pei-Zhi Zhuang

Corresponding author

E-mail: zhuangpeizhi@sdu.edu.cn

School of Qilu Transportation, Shandong University, Jinan, 250002, China

TS-PIELM: Physics-Informed Extreme Learning Machine Facilities Soil Consolidation Analyses

Authors: He **Yang**, Fei **Ren**, Hai-Sui **Yu**, Xueyu **Geng**, Pei-Zhi **Zhuang***

*Corresponding author: zhuangpeizhi@sdu.edu.cn

Abstract

Accuracy and efficiency of the conventional physics-informed neural network (PINN) need to be improved before it can be a competitive alternative for soil consolidation analyses. This paper aims to overcome these limitations by proposing a highly accurate and efficient physics-informed machine learning (PIML) approach, termed time-stepping physics-informed extreme learning machine (TS-PIELM). In the TS-PIELM framework the consolidation process is divided into numerous time intervals, which helps overcome the limitation of PIELM in solving differential equations with sharp gradients. To accelerate network training, the solution is approximated by a single-layer feedforward extreme learning machine (ELM), rather than using a fully connected neural network in PINN. The input layer weights of the ELM network are generated randomly and fixed during the training process. Subsequently, the output layer weights are directly computed by solving a system of linear equations, which significantly enhances the training efficiency compared to the time-consuming gradient descent method in PINN. Finally, the superior performance of TS-PIELM is demonstrated by solving three typical Terzaghi consolidation problems. Compared to PINN, results show that the computational efficiency and accuracy of the novel TS-PIELM framework are improved by more than 1000 times and 100 times for one-dimensional cases, respectively. This paper provides compelling evidence that PIML can be a powerful tool for computational geotechnics.

Keywords: consolidation, neural network, machine learning, physics-informed neural network, extreme learning machine, physics-informed extreme learning machine

1. Introduction

Consolidation of saturated soils is a time-dependent process in which excess water pressure gradually dissipates and the corresponding effective stress increases. Understanding soil consolidation behaviour is essential for the design, construction and maintenance of geo-structures such as embankment settlement, slope stability and underground deformation, where settlement and stability are key concerns. Terzaghi (1943) was the first to mathematically describe this process by proposing the well-known one-dimensional consolidation theory. Biot (1941) further developed a three-dimensional consolidation theory that incorporates hydro-mechanical coupling to account for both pore water flow and soil deformation. Nowadays, more advanced consolidation theories have been proposed for the analysis of complex soil consolidation behaviour, which are able to take more factors into account, such as nonlinear compressibility, creep behaviour, and unsaturated soil states (Yin and Graham 1989; Yin and Graham 1996; Xie et al. 2002; Chen and Yin 2023). On the other hand, the rapid evolution of consolidation theory poses challenges for theoretical analysis and numerical simulation as more complex consolidation equations need to be solved.

Analytical and numerical methods are commonly employed to solve the consolidation equations. However, very often analytical solutions are not easily available for high-dimensional consolidation problems with complex boundary conditions. Moreover, numerical simulations (e.g. the finite difference method and the finite element method) may suffer from mesh distortion, complex solution domains, complex boundary conditions, and low computational efficiency for inverse analyses, among others (Hu et al. 2024; Wang et al. 2024a; Wu et al. 2024). The recent development of physics-informed neural networks (PINN) has made it possible to solve ordinary differential equations (ODEs) and partial differential equations (PDEs) by implementing physical laws (Raissi et al. 2019; Karniadakis et al. 2021). Various differential equations can be solved with the universal function approximation capabilities of deep neural networks, and the mesh-free PINN can also mitigate issues related to mesh distortion. In geotechnical engineering, PINN has also been successfully applied to many problems such as Terzaghi's consolidation, hydro-mechanical coupling, thermo-mechanical coupling, cavity expansion theory, unsaturated soils, and finite element analysis (Zhou et al. ; Chen et al. 2024; Ouyang et al. 2024; Feng et al. 2025; Xu et al. 2025; Yang et al. 2025). Among these applications, the use of PINN for soil consolidation analyses has gained increasing attention in recent years (Mandl et al. 2023; Sadiku 2023; Guo and Yin 2024; Lan et al. 2024a; Lan et al. 2024b; Wang et al. 2024b;

Xie et al. 2024; Yuan et al. 2024; Zhang et al. 2024a; Zhang et al. 2024b; Zhou et al. 2025). These studies have made pioneering contributions to the application of PINN in geomechanics. It is necessary to mention that, however, the computational efficiency and accuracy of the current PINN techniques should be further improved. For example, conventional PINN techniques typically provide solution accuracy on the order of $10^{-2}\sim 10^{-4}$ in terms of absolute error, and the training time can be several minutes for one-dimensional consolidation problems or more than half an hour for high-dimensional cases after thousands of training epochs.

The multi-layered deep neural network and the time-consuming gradient descent methods for training network parameters are responsible for the low efficiency of conventional PINN. To improve training efficiency, an alternative is to replace fully connected neural networks with the extreme learning machine (ELM) (Huang et al. 2006), leading to the physics-informed extreme learning machine (PIELM) framework (Dwivedi and Srinivasan 2020). Compared to conventional PINN, there is only one hidden layer in the PIELM framework, whose input layer parameters are fixed during training and the output layer parameters are directly calculated with the Moore–Penrose generalized inverse. As a result, both the training efficiency and accuracy can be significantly improved in solving PDEs (Calabrò et al. 2021; Dong and Li 2021; Schiassi et al. 2021; Liu et al. 2023; De Florio et al. 2024). Despite these advantages, there are two main limitations that restrict the application of PIELM in geotechnical engineering:

- (a) PIELM can hardly handle those PDEs with sharp gradients, such as discontinuity between initial conditions and boundary conditions. This can be frequently met for soil consolidation analyses when the boundary loads are applied suddenly, which will conflict with the initial excess water distribution at the subjected boundaries. Hence, PIELM may fail to predict accurate consolidation solutions during the early dissipation period.
- (b) When calculating the Moore–Penrose generalized inverse, the computational cost increases exponentially. For high-dimensional consolidation problems, dealing with a large collection of training data can result in low training efficiency and excessive computational memory occupation.

Overall, given the significant potential of PIELM, further improvements are essential to advance its application in soil consolidation analyses and broader geotechnical engineering problems. To fill the gap, this paper proposes an accurate, efficient, and robust time-stepping PIELM (TS-PIELM) to solve Terzaghi

consolidation equations. While retaining the key advantages of the PIELM, the TS-PIELM can effectively overcome the two major limitations, thereby facilitating soil consolidation analyses. The rest part of this paper is organised as follows. First, the governing equations as well as initial and boundary conditions are shown in a general form for consolidation analyses, and a conventional PINN framework for solving the consolidation equations is introduced. Then the PIELM and TS-PIELM frameworks are detailed. Later, the performance of TS-PIELM is tested using 3 case studies. Finally, the applications of the TS-PIELM approach in solving consolidation problems are discussed and main conclusions are drawn.

2. Overview of Terzaghi's Consolidation Theory and PINN framework

Before showing the PIELM framework, the governing equations and the PINN framework for Terzaghi's consolidation theory are described briefly at first.

2.1. Problem definition of Terzaghi's consolidation theory

In Terzaghi consolidation theory, it is assumed that soil particles are incompressible and the dissipation of excess water pressure follows Darcy's law. The volume change of saturated soil is solely attributed to the net flow of pore water. Within a solution domain Ω , the consolidation problem is governed by the following equations, along with the corresponding initial and boundary conditions:

$$\frac{\partial u(\mathbf{x}, t)}{\partial t} - c \nabla^2 u(\mathbf{x}, t) = 0, \quad \mathbf{x} \in \Omega, t \in [0, T] \quad (1)$$

$$u(\mathbf{x}, 0) = u_0(\mathbf{x}), \quad \mathbf{x} \in \Omega \quad (2)$$

$$\mathcal{B}[u(\mathbf{x}, t)] = h(\mathbf{x}, t), \quad \mathbf{x} \in \partial\Omega, t \in [0, T] \quad (3)$$

where $u(\mathbf{x}, t)$ is the excess pore water pressure, which is the function of spatial variable \mathbf{x} and time t ; c denotes the consolidation coefficient; ∇^2 is the Laplace operator; $u_0(\mathbf{x})$ is the initial excess water pressure; $\mathcal{B}[\cdot]$ denotes the operator for Dirichlet/Neumann boundary conditions. It is also worth emphasizing that in Eq. (1) the soil is assumed to be isotropic, meaning its vertical and horizontal consolidation coefficients are identical. This study focuses on solving consolidation equations by physics-informed machine learning (PIML) techniques, and therefore, the validity and soundness of these equations are beyond the scope of this work.

2.2. PINN framework for consolidation analyses

PINN approximates the exact solutions for PDEs by a neural network architecture, as shown in Figure 1. The spatial and temporal coordinates, \mathbf{x} and t , are fed into the input layer, and the trial function $u(\mathbf{x}, t)$ is obtained after propagating through multiple hidden layers. The predicted $u(\mathbf{x}, t)$ is then substituted into the physical laws to compute the residuals, which define the overall loss function as follows:

$$\mathcal{L}(\boldsymbol{\theta}) = \lambda_{\text{pde}} \mathcal{L}_{\text{pde}}(\boldsymbol{\theta}) + \lambda_{\text{bc}} \mathcal{L}_{\text{bc}}(\boldsymbol{\theta}) + \lambda_{\text{ic}} \mathcal{L}_{\text{ic}}(\boldsymbol{\theta}) \quad (4)$$

$$\mathcal{L}_{\text{pde}}(\boldsymbol{\theta}) = \frac{1}{N_c} \sum_{i=1}^{N_c} \left| \frac{\partial u}{\partial t}(\mathbf{x}_i, t_i; \boldsymbol{\theta}) - c \nabla^2 u(\mathbf{x}_i, t_i; \boldsymbol{\theta}) \right|^2 \quad (5)$$

$$\mathcal{L}_{\text{bc}}(\boldsymbol{\theta}) = \frac{1}{N_B} \sum_{j=1}^{N_B} \left| \mathcal{B}[u(\mathbf{x}_j, t_j)] - h(\mathbf{x}_j, t_j) \right|^2 \quad (6)$$

$$\mathcal{L}_{\text{ic}}(\boldsymbol{\theta}) = \frac{1}{N_I} \sum_{l=1}^{N_I} \left| u(\mathbf{x}_l, 0; \boldsymbol{\theta}) - u_0(\mathbf{x}_l) \right|^2 \quad (7)$$

where \mathcal{L}_{pde} , \mathcal{L}_{bc} , and \mathcal{L}_{ic} are loss terms related to the governing PDEs, initial conditions and boundary conditions, respectively; λ_{pde} , λ_{bc} and λ_{ic} are the weights of corresponding loss terms; $\boldsymbol{\theta}$ denotes the network parameters. In Eqs. (5), (6) and (7), $\{\mathbf{x}_i, t_i\}_{i=1}^{N_c}$ are the training points in the solution region Ω , $\{\mathbf{x}_j, t_j\}_{j=1}^{N_B}$ are the points on the boundaries of the solution region, and $\{\mathbf{x}_l, 0\}_{l=1}^{N_I}$ are the training points generated from initial conditions. The involved partial derivatives in the loss function can be calculated using automatic differentiation (AD). Later, the total loss is minimised by gradient descent methods, and the network parameters $\boldsymbol{\theta}$ are updated epoch by epoch until convergence is reached. Finally, the trained neural network can provide an approximate consolidation solution with the input of (\mathbf{x}, t) . To further improve solution accuracy, hard constraints can be embedded into the framework, enabling the initial/boundary conditions to be automatically satisfied (Lu et al. 2021; Schiassi et al. 2021; Lan et al. 2024a; Zhang et al. 2024a).

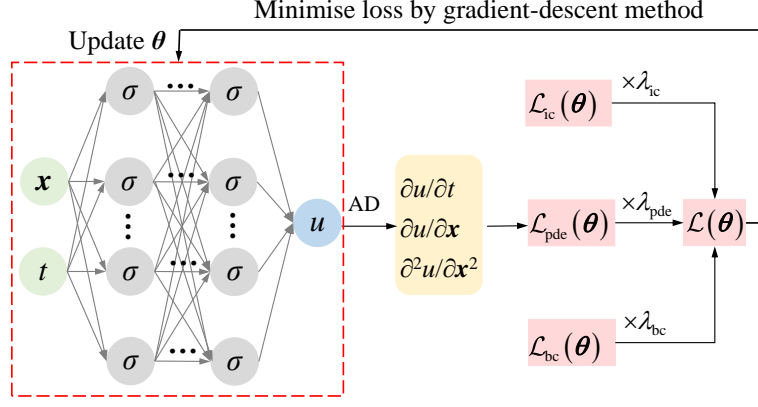


Figure 1. PINN framework for consolidation analysis

3. PIELM and TS-PIELM framework for Consolidation Analyses

In this section the PIELM and TS-PIELM frameworks for solving consolidation problems are detailed, highlighting how to improve the performance of conventional PINN by replacing deep neural networks with ELM.

3.1. Physics-informed extreme learning machine

In order to abandon the time-consuming gradient descent methods in network training, the PIELM framework finds the latent consolidation solution θ using ELM instead of fully connected neural networks. As illustrated in Figure 2, there is only one hidden layer in the ELM network with dozens of neurons. The input layer parameters are randomly initialised within the range of $[-1, 1]$ and remain fixed throughout training. The output layer parameters are directly determined by minimising the loss vector (physical information at each collocation point), defined as:

$$\left[\mathcal{L}_{\text{pde}}^{(1)}(\theta), \dots, \mathcal{L}_{\text{pde}}^{(N_c)}(\theta), \mathcal{L}_{\text{bc}}^{(1)}(\theta), \dots, \mathcal{L}_{\text{bc}}^{(N_B)}(\theta), \mathcal{L}_{\text{ic}}^{(1)}(\theta), \dots, \mathcal{L}_{\text{ic}}^{(N_l)}(\theta) \right] \rightarrow \mathbf{0} \quad (8)$$

$$\mathcal{L}_{\text{pde}}^{(i)}(\theta) = \frac{\partial u}{\partial t}(\mathbf{x}_i, t_i; \theta) - c \nabla^2 u(\mathbf{x}_i, t_i; \theta) \quad i = 1, 2, \dots, N_c \quad (9)$$

$$\mathcal{L}_{\text{bc}}^{(j)}(\theta) = \mathcal{B} \left[u(\mathbf{x}_j, t_j) \right] - h(\mathbf{x}_j, t_j) \quad j = 1, 2, \dots, N_B \quad (10)$$

$$\mathcal{L}_{\text{ic}}^{(l)}(\theta) = u(\mathbf{x}_l, 0; \theta) - u_0(\mathbf{x}_l) \quad l = 1, 2, \dots, N_l \quad (11)$$

where θ denotes the output layer parameters in ELM networks and can be directly solved by the least squares method with the Moore–Penrose generalised inverse. Then the solution for Terzaghi consolidation problems can be obtained by the trained ELM. Compared to the PINN employing the time-consuming gradient descent

method, the PIELM framework can directly calculate the network parameters to reduce the training cost.

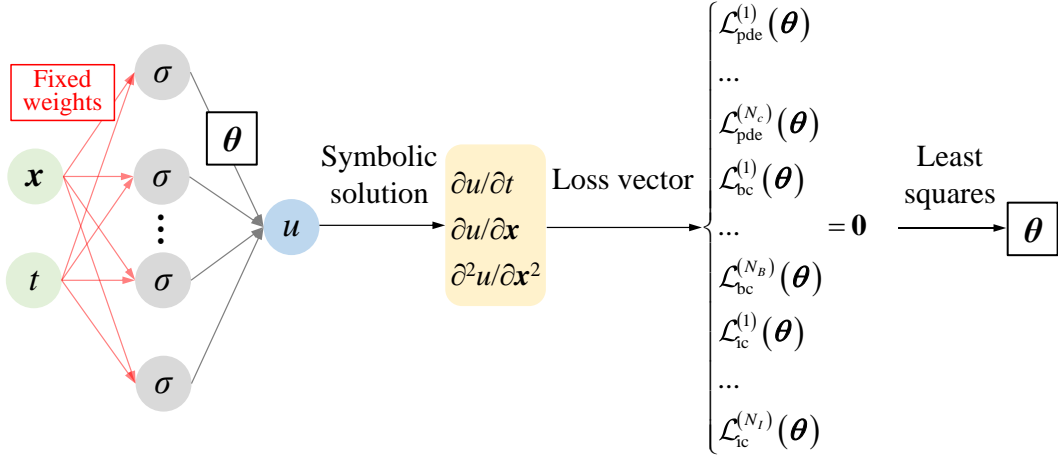


Figure 2. PIELM framework for consolidation analysis

3.2. Time-stepping physics-informed extreme learning machine

In the standard PIELM framework, time is treated as a continuous input into the ELM network, yielding $u(x, t)$ as the function of x and t . In contrast, the TS-PIELM utilises discretized time formulation, as described below.

The consolidation process is divided into a number of time intervals that can either be of equal or varying lengths. Taking equal-length intervals as an example, the consolidation equation (1) can be written in the Crank–Nicolson discrete form as

$$u_{k+1}(\mathbf{x}) = u_k(\mathbf{x}) + \frac{\Delta t}{2} c \left[\nabla^2 u_{k+1}(\mathbf{x}) + \nabla^2 u_k(\mathbf{x}) \right] \quad (12)$$

where Δt denotes the time interval; u_k denotes the excess water pressure when $t = t_k = k\Delta t$ ($k=0, 1, 2, \dots$). The TS-PIELM architecture for solving the consolidation equations is shown in Figure 3. Different from the standard PIELM framework, a separate ELM network is required at each time step. The output u_k from the k -th ELM network will serve as the initial conditions for the $(k+1)$ -th ELM network. Letting $u_k(\mathbf{x}; \theta_k) = u(\mathbf{x}, t_k)$ and θ_k denotes the weight parameters of k -th network, the loss vector at the $(k+1)$ -th incremental step will be

$$\mathcal{L}(\theta_{k+1}) = \left[\mathcal{L}_{\text{pde}}^{(1)}(\theta_{k+1}), \dots, \mathcal{L}_{\text{pde}}^{(N_c)}(\theta_{k+1}), \mathcal{L}_{\text{bc}}^{(1)}(\theta_{k+1}), \dots, \mathcal{L}_{\text{bc}}^{(N_B)}(\theta_{k+1}) \right] \rightarrow \mathbf{0} \quad (13)$$

$$\mathcal{L}_{\text{pde}}^{(i)}(\theta_{k+1}) = u_{k+1}(\mathbf{x}_i; \theta_{k+1}) - \frac{\Delta t}{2} c \left[\nabla^2 u_{k+1}(\mathbf{x}_i; \theta_{k+1}) + \nabla^2 u_k(\mathbf{x}_i; \theta_k) \right] - u_k(\mathbf{x}_i; \theta_k) \quad (14)$$

$$\mathcal{L}_{\text{bc}}^{(i)}(\theta_{k+1}) = \mathcal{B} \left[u_{k+1}(\mathbf{x}_j; \theta_{k+1}) \right] - h(\mathbf{x}_j) \quad (15)$$

Following a similar procedure of PIELM in Section 3.1, θ_{k+1} can be readily calculated by optimising

$\mathcal{L}(\theta_{k+1})=0$. Subsequently, $u_{k+1}(\mathbf{x}; \theta_{k+1})$ can be determined by the trained ELM network, and $u(\mathbf{x}, t)$ can be computed step by step by increasing k . It can be found that the TS-PIELM requires computing the Moore-Penrose inverse at each time step rather than over the whole dissipation period. In the next sections, the advantages of this discrete method will be demonstrated by case studies.

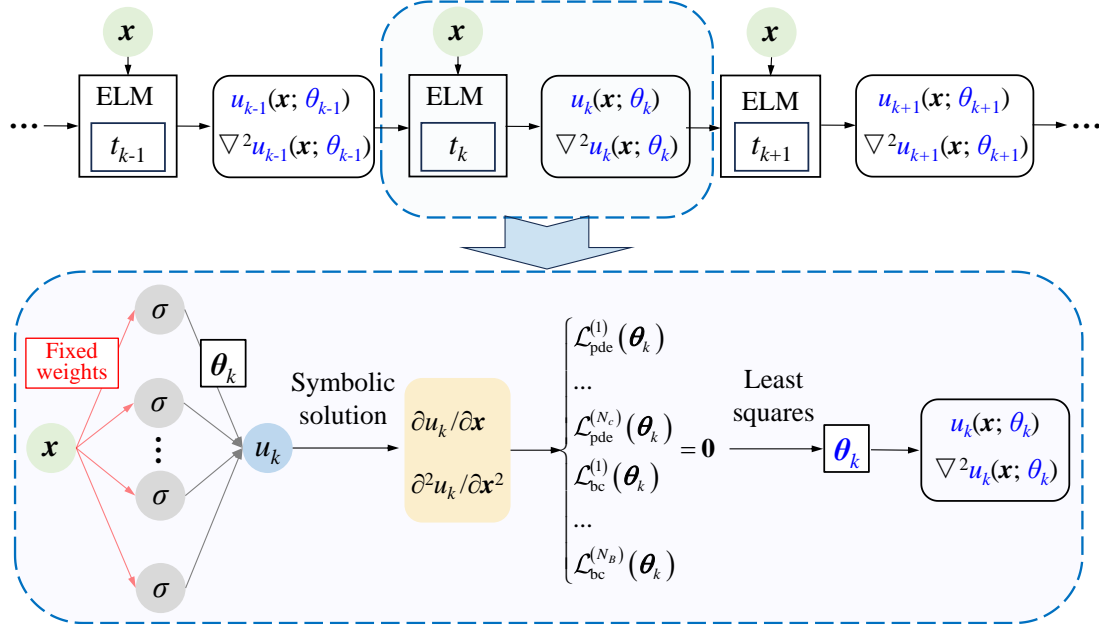


Figure 3. TS-PIELM framework for consolidation analysis

4. Performance of TS-PIELM

The superior performance of the proposed TS-PIELM framework is demonstrated using three representative consolidation cases with well-established analytical solutions, including two one-dimensional and one two-dimensional consolidation problems. Note that the mesh-free TS-PIELM can deal with consolidation equations with various initial and boundary conditions, but only cases with analytical solutions are chosen to rigorously quantify the high accuracy of TS-PIELM against exact benchmarks (e.g., the point-wise error can be less than 10^{-6}). For comparison, results obtained from PINN and standard PIELM are also presented. All simulations are conducted using MATLAB R2023b on a Dell Precision 7960 workstation, equipped with an Intel Xeon W7-3445 (2.59 GHz) processor and 64GB of RAM. The hyperparameters of the neural networks as well as training details are summarised in Table 1. Following Lu et al. (2021), Schiassi et al. (2021), and Lan et al. (2024a), hard constraints are imposed on the governing equations and boundary conditions in TS-PIELM, PIELM and PINN. The corresponding constrained expressions are provided in the Appendix. Furthermore, since the training efficiency of PINN depends on the weighting of different loss terms (e.g., Eq.

(4)), a self-adaptive loss balancing technique based on maximum likelihood estimation is introduced to dynamically update loss weights at each training epoch (Xiang et al. 2022). To assess the predictive accuracy, the relative L_2 error is defined as follows:

$$L_2 = \frac{\sqrt{\sum_1^N (\text{exact} - \text{predicted})^2}}{\sqrt{\sum_1^N (\text{exact})^2}} \quad (16)$$

where N is the number of test points.

Table 1 Summary of hyperparameters and training information

Cases	Case 1			Case 2			Case 3		
Frameworks	TS-PIELM	PIELM	PINN	TS-PIELM	PIELM	PINN	TS-PIELM	PIELM	PINN
	20	100	64*3	20	100	64*3	150	1000	64*3
Activation function	tanh	tanh	tanh	tanh	tanh	tanh	tanh	tanh	tanh
N_c	1000	2000	2000	1000	2000	2000	10000	20000	20000
N_I	-	100	100	-	100	100		2000	2000
Time-interval (s)	0.001	-	-	0.001			0.01		
Training time (s)	0.37	0.86	434.10	0.34	0.99	405.41	10.14	47.82	5231.85
L_2	2.94e-04	5.92e-2	3.28e-2	4.90e-04	1.48e-2	0.0213	2.50e-3	9.32e-2	9.43e-2

Note: For PINN, epoch=5000; initial learning rate=0.001; decay rate=0.005

4.1. One-dimensional consolidation in Certain coordinates

The proposed TS-PIELM approach is first tested by a one-dimensional vertical consolidation problem, which serves as a well-established benchmark for assessing the performance of PINN in consolidation analysis. Within the solution domain of $0 < z < H$, the top boundary ($z=0$) is a drainage outlet and the bottom boundary ($z=H$) is impermeable. The excess pore water pressure $u(z,t)$ is governed by

$$\begin{cases} \frac{\partial u}{\partial t} = c \frac{\partial^2 u}{\partial z^2} \\ u(z, 0) = p_0 \\ u(0, t) = 0 \\ \left. \frac{\partial u}{\partial z} \right|_{z=H} = 0 \end{cases} \quad (17)$$

where p_0 is the initial uniform excess water pressure; H is the vertical distance from the top to the bottom boundary. The exact solution of Eq. (17) and the dimensionless time (T) are expressed as

$$\frac{u(z, t)}{p_0} = \frac{4}{\pi} \sum_{n=1}^{\infty} \frac{1}{(2n+1)} \sin \left[\frac{(2n+1)\pi z}{2H} \right] \exp \left[-\frac{(2n+1)^2 \pi^2 ct}{4H^2} \right] \quad (18)$$

$$T = ct/H^2 \quad (19)$$

Figure 4 compares the predicted $u(z, t)$ by PIML approaches against the exact solution at various consolidation times (i.e. $T=0.001, 0.01, 0.1, 0.5, 1$). It shows that the TS-PIELM results agree well with the exact solution, providing the relative L_2 error of $2.94e-04$. In contrast, both PIELM and PINN predict reasonable results for longer consolidation time (e.g., $T \geq 0.01$), but fail to provide accurate predictions of $u(z, t)$ when the consolidation time is short (e.g., $T < 0.01$). As shown in Table 1, the relative L_2 error for PIELM and PINN are $5.92e-2$ and $3.28e-2$, respectively, indicating that the TS-PIELM approach can increase accuracy by more than 100 times. Regarding computational efficiency, PINN requires the highest training time (more than 1000 times compared to TS-PIELM) due to the inherent limitations of deep neural networks, and the training time for TS-PIELM and PIELM is significantly reduced after incorporating ELM networks. Notably, the training time for TS-PIELM is only half of that for PIELM, primarily because fewer hidden layer neurons and training data are required at each step.

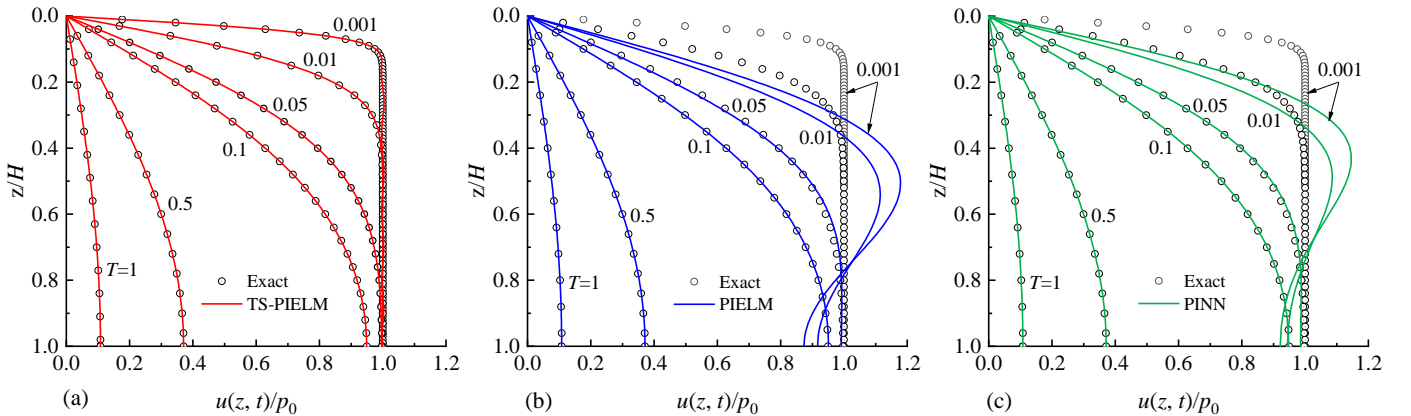


Figure 4. Comparison of excess pore water pressures predicted by PIML against the exact solution

To further emphasize the higher accuracy of the novel TS-PIELM method, contour plots of the absolute point-wise errors (i.e., absolute value of the predicted minus the exact u/p_0) are shown in Figure 5. It can be found that:

- (a) When $0 < T < 0.01$, the absolute error for TS-PIELM ranges between 10^{-5} and 10^{-2} , but it sharply decreases to below 10^{-5} when $T > 0.01$. The smoothness of the error surface indicates the robustness of the TS-PIELM.
- (b) The absolute errors for both PIELM and PINN remain below 1 and then decrease to the order of 10^{-4} when $T > 0.05$. The error surfaces are uneven, indicating their lower robustness.
- (c) Overall, the relative L_2 error is mainly affected by the predictions at $T < 0.01$. This is because, when $t=0$, the initial conditions do not align with the boundary conditions at $z=0$, and the gradient of $u(z, t)$ becomes excessively steep for a small T , leading to higher errors.

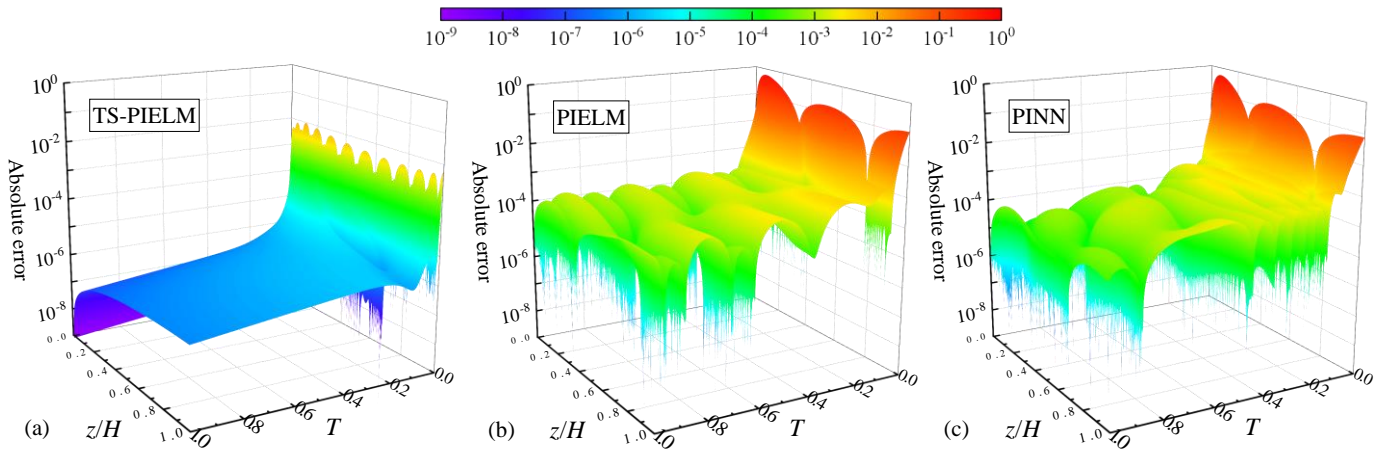


Figure 5. Absolute error contours of u/p_0 for TS-PIELM, PIELM and PINN

4.2. One-dimensional radial consolidation

The second illustrative case is a one-dimensional radial consolidation problem defined within the domain range of $a < r < b$, where the boundary $r=a$ is permeable and the boundary $r=b$ is subjected to constant pressure p_0 representing a far zone. In this case, $u(r,t)$ is governed by

$$\begin{cases} \frac{\partial u}{\partial t} = c \left(\frac{\partial^2 u}{\partial r^2} + \frac{1}{r} \frac{\partial u}{\partial r} \right) \\ u(r, 0) = p_0 \\ u(a, t) = 0 \\ u(b, t) = p_0 \end{cases} \quad (20)$$

The analytical solution can be found in Carslaw and Jaeger (1947) and Yang et al. (2024), and it can be expressed as

$$\frac{u}{p_0} = 1 - \frac{\ln(b/r)}{\ln(b/a)} - \pi \sum_{n=1}^{\infty} \frac{J_0(\beta_n a) J_0(\beta_n b) U_0(\beta_n r)}{J_0^2(\beta_n a) - J_0^2(\beta_n b)} \exp(-c \beta_n^2 t) \quad (21)$$

$$U_0(\beta_n r) = J_0(\beta_n r) Y_0(\beta_n b) - J_0(\beta_n b) Y_0(\beta_n r) \quad (22)$$

where J_0 and Y_0 are the first and second kinds of Bessel functions of zero order, respectively; α_n is the n -th root of $U_0(\alpha_n a) = 0$. For this case, the dimensionless time is defined as $T = ct/a^2$.

Figure 6 shows the comparison of $u(r, t)$ between the exact solution and predicted results by the three PIML approaches, plotted on a semi-logarithmic scale. Once again, TS-PIELM demonstrates an excellent agreement with the exact solution, whereas both PIELM and PINN fail to provide acceptable predictions when $T < 0.01$. Also, the training time and relative L_2 error for TS-PIELM (0.34s and 4.90e-4) is approximately 1/3 and 1/30 of those for PIELM, respectively. The absolute error contours of u/p_0 are plotted in Figure 7 and further validate the superior accuracy of TS-PIELM in this case.

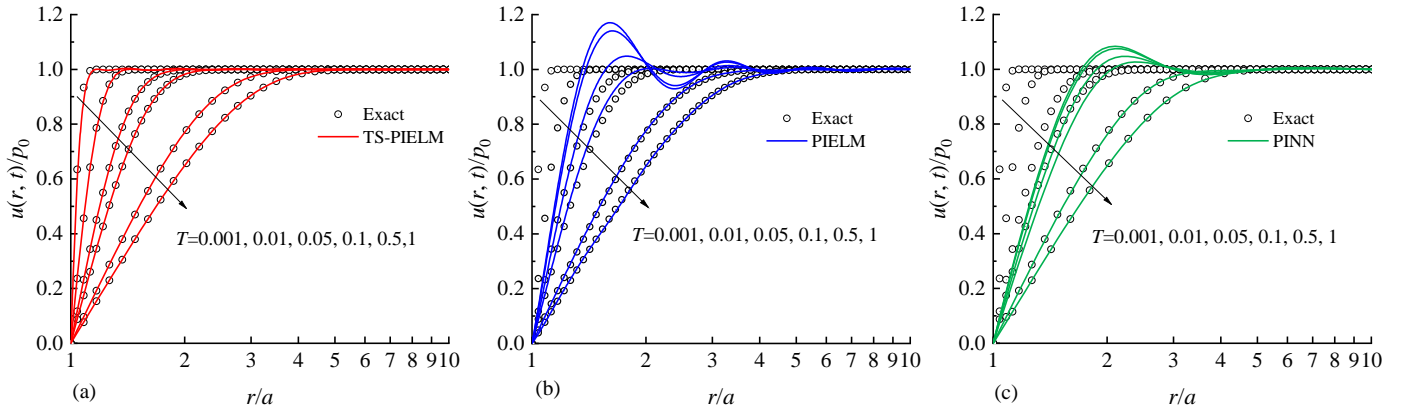


Figure 6. Comparison of excess pore water pressures predicted by PIML against the exact solution

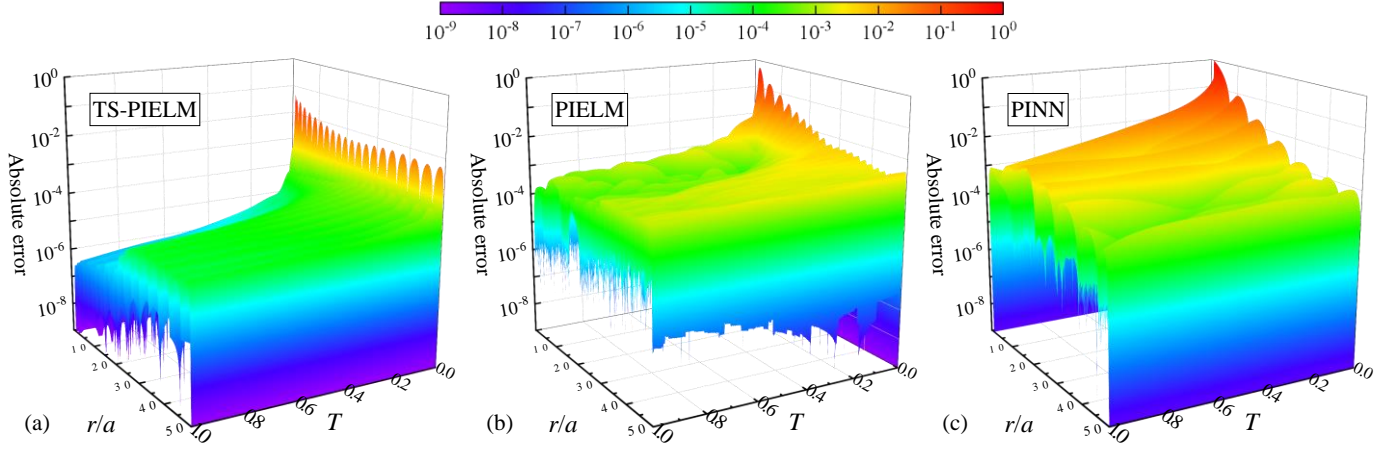


Figure 7. Absolute error contours of u/p_0 for TS-PIELM, PIELM and PINN

4.3. Two-dimensional radial consolidation with vertical drains

The final case study examines two-dimensional radial consolidation with prefabricated vertical drains (PVDs), a widely adopted technique to enhance drainage and accelerate soft clay consolidation. (Indraratna et al. 2009; Geng and Yu 2017; Ni et al. 2022). As shown in Figure 8, within the solution domain of $a < r < b$ and $0 < z < H$, the problem is defined by Eq. (23):

$$\begin{cases}
 \frac{\partial u}{\partial t} = c \left(\frac{\partial^2 u}{\partial r^2} + \frac{1}{r} \frac{\partial u}{\partial r} + \frac{\partial^2 u}{\partial z^2} \right) \\
 u(r, z, 0) = p_0 \\
 u(a, z, t) = 0 \\
 \left. \frac{\partial u}{\partial r} \right|_{r=b} = 0 \\
 u(r, 0, t) = 0 \\
 \left. \frac{\partial u}{\partial z} \right|_{z=H} = 0
 \end{cases} \quad (23)$$

The analytical solution of Eq. (23) can be expressed as

$$\frac{u(r, z, t)}{p_0} = F_r F_z \quad (24)$$

$$F_z = \frac{4}{\pi} \sum_{n=1}^{\infty} \frac{1}{(2n+1)} \sin\left(\frac{(2n+1)\pi z}{2H}\right) \exp\left(-\frac{(2n+1)^2 \pi^2 ct}{4H^2}\right) \quad (25)$$

$$F_r = \sum_{n=1}^{\infty} \frac{\int_a^b U(r) r dr}{\int_a^b U^2(r) r dr} U(r) \exp(-c\beta_n^2 t) \quad (26)$$

$$U(r) = Y_0(\beta_n r) - \frac{Y_0(\beta_n a)}{J_0(\beta_n a)} J_0(\beta_n r) \quad (27)$$

where β_n is the n-th root of the $J_0(\beta a)Y_1(\beta b) - Y_0(\beta a)J_1(\beta b) = 0$, where Y_1 and J_1 are the first and second kinds of Bessel functions of first order, respectively.

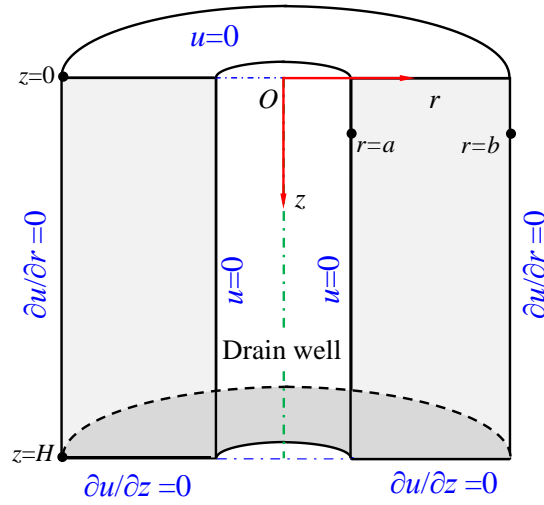


Figure 8. Schematic of radial consolidation with prefabricated vertical drain

In this case the PVD sizes are set as $a=0.07\text{m}$ and $b=0.7\text{m}$ (Geng and Yu 2017), and the dimensionless time is defined as $T = ct/H^2$ where $H=5\text{m}$. [Figure 9](#) and [Figure 10](#) show the predicted $u(r, z, t)/p_0$ and absolute point-wise error on different occasions, respectively, and only the results predicted by TS-PELEM and PIELM are shown to save paper length. Owing to more training points and hidden layer neurons required in ELM networks, the training time for TS-PIELM and PIELM increased to 10s and 48s, respectively, which is significantly lower than that of PINN after 5000 epochs (over 1 hour). As shown by the contour plots of u/p_0 and absolute error, TS-PIELM can accurately predict the pore water pressure evolution in this two-dimensional consolidation problem with discontinuous initial and boundary conditions at two boundaries ($z=0$ and $r=a$), giving the relative L_2 error of $2.50\text{e-}3$. Nevertheless, PIELM performs worse in terms of both relative L_2 error and absolute error, especially when $T < 4\text{e-}3$ (i.e., $ct < 0.1\text{m}^2$). Overall, the superior performance of TS-PIELM has been further demonstrated.

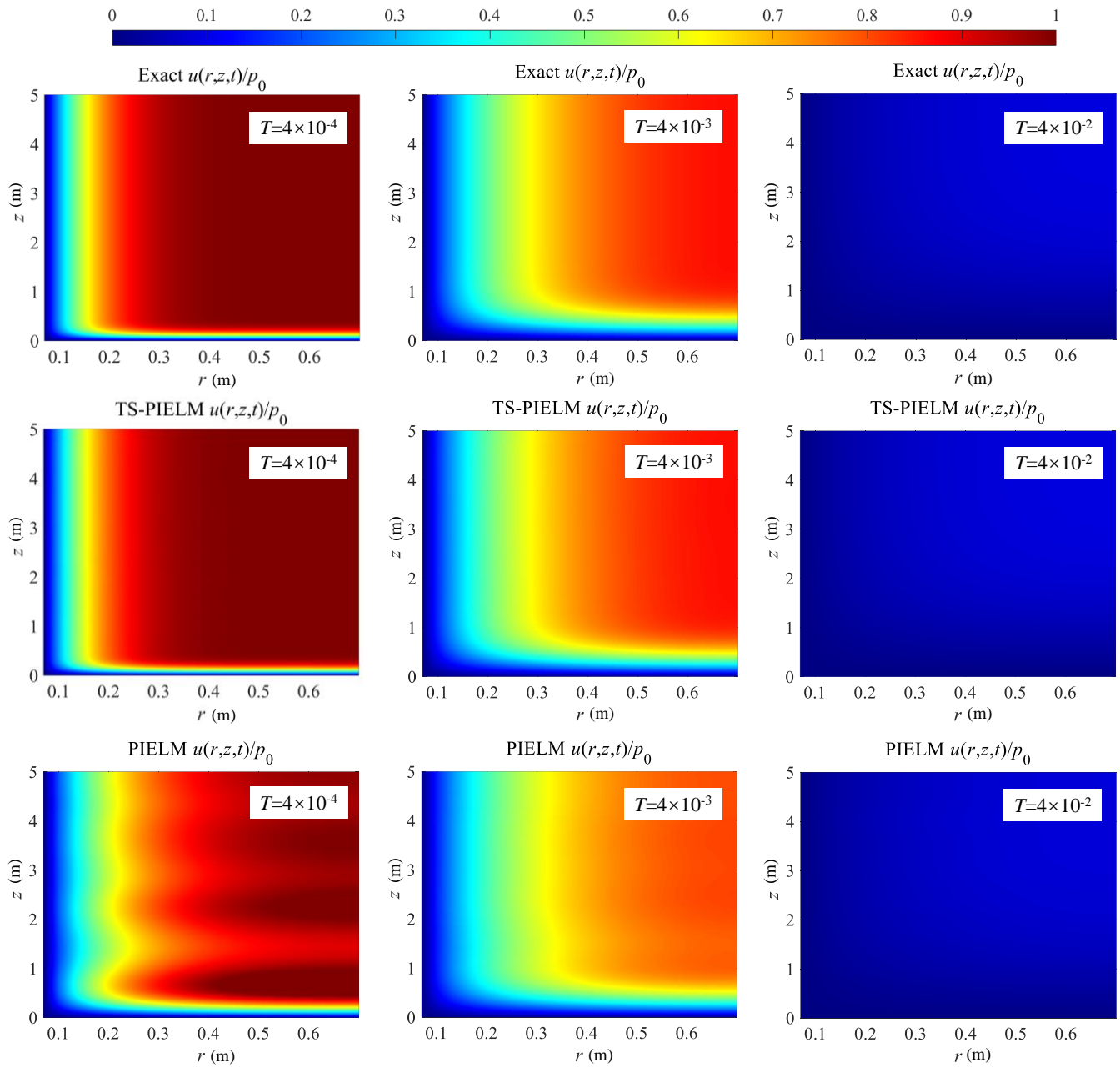


Figure 9. Excess pore water pressures predicted by TS-PIELM and PIELM against the exact solution

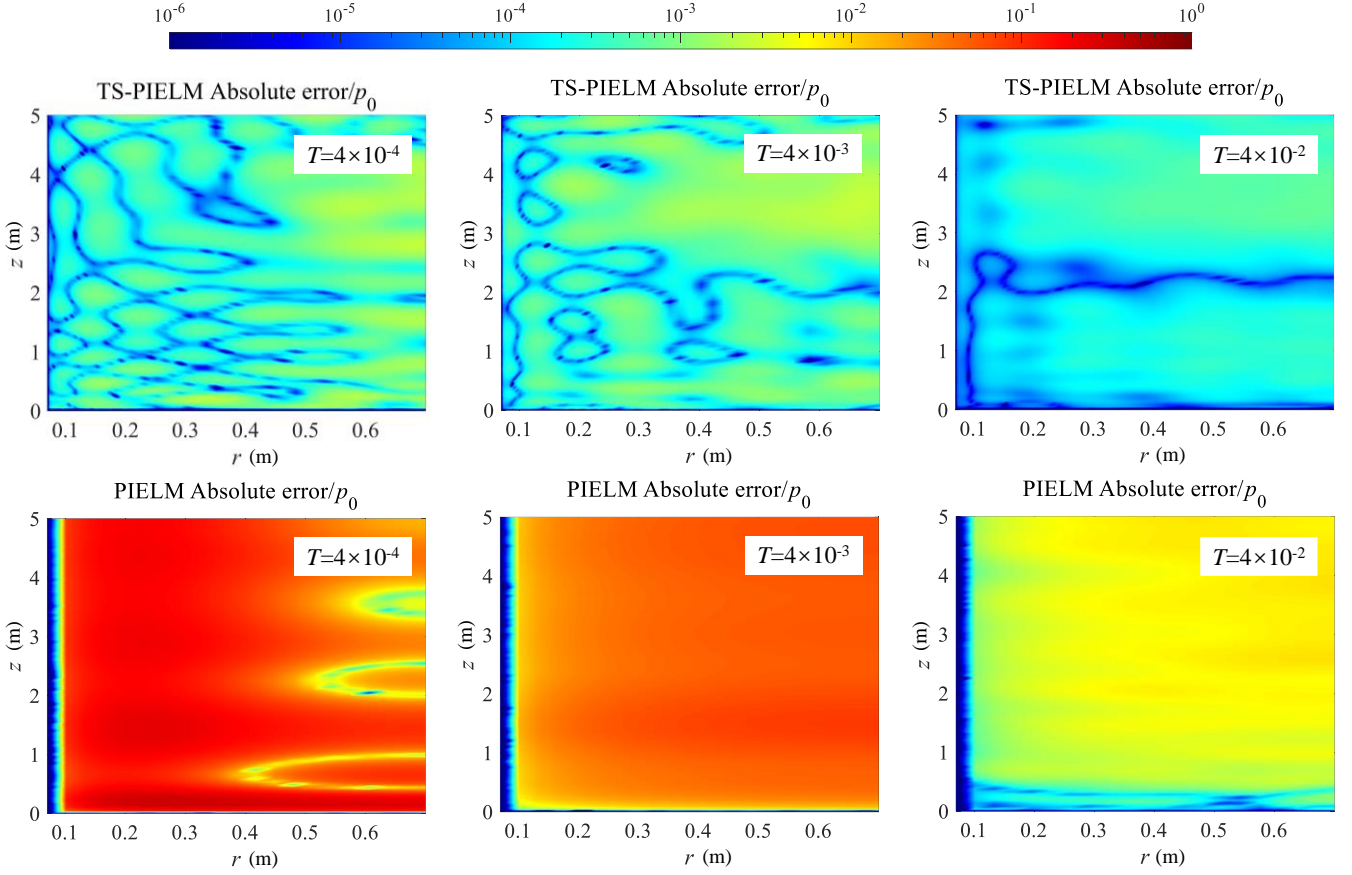


Figure 10. Absolute error of u/p_0 for TS-PIELM and PIELM

5. Discussion

After showing the performance of the three PIML approaches, this section primarily discusses the advantages and limitations of the proposed TS-PIELM approach:

- (a) Firstly, the higher efficiency, accuracy and robustness of the TS-PIELM are mainly attributed to the ELM network whose model weights are much easier to be determined. This also explains why the efficiency of PIELM and TS-PIELM are superior to PINN which requires significantly more time to train model parameters.
- (b) Secondly, the TS-PIELM adopts discrete time intervals instead of continuous time input. This approach reduces memory usage and enhances efficiency, as fewer training points and hidden layer neurons are required for training ELM networks. This can be more significant for solving high-dimensional consolidation problems.
- (c) When the initial conditions and boundary conditions do not match at some boundaries, PIELM encounters difficulties in handling such PDEs with sharp gradients. Increasing the amount of training data may help smooth the gradient, but calculating the Moore–Penrose generalised inverse involves

high memory usage and extensive computation time. The proposed TS-PIELM provides a new way to solve such problems by smoothing the sharp change in excess water pressure via the time-stepping method.

While the advantages of TS-PIELM are shown, there may also be some limitations. The dissipation rate of pore water pressure normally decreases as the pressure gradient decreases with time. The training efficiency of TS-PIELM can be further improved using unequal time intervals. For instance, self-adaptive methods can be incorporated into TS-PIELM to dynamically generate time intervals. Moreover, the training results of TS-PIELM are dependent on the training data distributions, training data number and hidden layer neurons. In the future, error estimation, probability analysis and definition of assessment indicators are necessary to enhance the explainability of TS-PIELM in solving equations.

6. Conclusions

This paper proposes a highly accurate and efficient TS-PIELM framework to facilitate soil consolidation analyses. In the TS-PIELM framework, the consolidation process is divided into a number of incremental time steps. The neural network is trained at each time step, and the fully connected neural network is replaced by an extreme learning machine (ELM). There is only one single hidden layer in the ELM network, and a loss vector can be formed by incorporating the consolidation equations as well as initial and boundary conditions. The input layer weights are generated randomly, and the output layer weights are directly calculated by minimising the loss vector. When compared to PINN, which trains neural networks by the time-consuming gradient descent method, the efficiency of TS-PIELM is significantly improved by training the ELM network using the least squares method. Compared to PIELM, the time-stepping technique in the TS-PIELM framework further enhances solution accuracy, efficiency and robustness after mitigating sharp gradients and reducing the amount of training data. Finally, the superior performance of PIELM is demonstrated by three consolidation problems. For the one-dimensional cases, the TS-PIELM network training takes less than 0.5s, and its accuracy is improved by at least two orders of magnitude compared to PIELM and PINN. For the two-dimensional case, TS-PIELM improves the efficiency and accuracy by factors of more than 5000 and 30, respectively, compared to PINN. This paper provides timely evidence that physics-informed machine learning can be a powerful tool for computational geotechnics, and the novel method can also be applied to solve other

Appendix Constrained expressions in case studies

To improve the accuracy of PIML, the network architecture can be modified by applying hard constraints, which ensure that initial/boundary conditions are strictly satisfied (Lu et al. 2021; Schiassi et al. 2021; Lan et al. 2024a; Zhang et al. 2024a). Following Schiassi et al. (2021), the solution of the PDE to be determined can be written in a constrained expression comprising:

- (a) a function that analytically satisfies the constraints;
- (b) a functional comprising a free function $g(\mathbf{x}, t)$ that is approximated by the deep neural network in PINN and by the ELM in PIELM.

The constrained expression represents the family of all possible functions that satisfy the constraints, transforming constrained problems into unconstrained problems. For the three case studies in this paper, the initial and boundary conditions do not exactly match each other. Hence, the hard constraints are only applied to the boundary conditions, and the constrained expressions are summarised in this appendix. The detailed method for constructing the expressions can be found in Schiassi et al. (2021) and is not repeated here.

In Case 1, the constrained expression is

$$u(z, t) = g(z, t) - g(0, t) - z(\partial g / \partial z) \Big|_{z=H} \quad (28)$$

In Case 2, the constrained expression is

$$u(r, t) = g(r, t) - \frac{r-b}{a-b} g(a, t) + \frac{r-a}{a-b} [g(b, t) - p_0] \quad (29)$$

Finally, in Case 3, the constrained expression is

$$\begin{aligned} u(r, z, t) = & g(r, z, t) - g(a, z, t) - (r-a)(\partial g / \partial r) \Big|_{r=b} \\ & - g(r, 0, t) + g(a, 0, t) + (r-a)(\partial g / \partial r) \Big|_{z=0} \\ & - z g_z(r, H, t) + z g_z(a, H, t) + (r-a) z (\partial^2 g / \partial r \partial z) \Big|_{r=b, z=H} \end{aligned} \quad (30)$$

Data Available Statement

Data will be available from the corresponding author upon reasonable request.

Conflict of interests

The authors declare that there is no known conflict of interest.

References

- Biot, M. A. (1941). "General Theory of Three - Dimensional Consolidation." Journal of Applied Physics **12**: 155-164.
- Carslaw, H. S. and Jaeger, J. C. (1947). Conduction of heat in solids. Oxford, The Clarendon Press.
- Chen, X.-X., Zhang, P., Yu, H.-S., Yin, Z.-Y. and Sheil, B. (2024). "Parsimonious Universal Function Approximator for Elastic and Elasto-Plastic Cavity Expansion Problems." ArXiv **abs/2407.19074**.
- Chen, Z.-J. and Yin, J.-H. (2023). "A New One-Dimensional Thermal Elastic-Viscoplastic Model for the Thermal Creep of Saturated Clayey Soils." Journal of Geotechnical and Geoenvironmental Engineering **149**(4): 04023010.
- Dwivedi, V. and Srinivasan, B. (2020). "Physics Informed Extreme Learning Machine (PIELM)–A rapid method for the numerical solution of partial differential equations." Neurocomputing **391**: 96-118.
- Feng, Y., Eun, J., Kim, S. and Kim, Y.-R. (2025). "Application of physics-informed neural networks (PINNs) solution to coupled thermal and hydraulic processes in silty sands." International Journal of Geo-Engineering **16**(1): 1-18.
- Geng, X. and Yu, H.-S. (2017). "A large-strain radial consolidation theory for soft clays improved by vertical drains." Géotechnique **67**(11): 1020-1028.
- Guo, H. and Yin, Z.-Y. (2024). "A novel physics-informed deep learning strategy with local time-updating discrete scheme for multi-dimensional forward and inverse consolidation problems." Computer Methods in Applied Mechanics and Engineering **421**: 116819.
- Hu, H., Qi, L. and Chao, X. (2024). "Physics-informed Neural Networks (PINN) for computational solid mechanics: Numerical frameworks and applications." Thin-Walled Structures: 112495.

- Huang, G.-B., Zhu, Q.-Y. and Siew, C.-K. (2006). "Extreme learning machine: Theory and applications." Neurocomputing **70**(1): 489-501.
- Indraratna, B., Attya, A. and Rujikiatkamjorn, C. (2009). "Experimental investigation on effectiveness of a vertical drain under cyclic loads." Journal of geotechnical and geoenvironmental engineering **135**(6): 835-839.
- Karniadakis, G. E., Kevrekidis, I. G., Lu, L., Perdikaris, P., Wang, S. and Yang, L. (2021). "Physics-informed machine learning." Nature Reviews Physics **3**(6): 422-440.
- Lan, P., Su, J.-j., Ma, X.-y. and Zhang, S. (2024a). "Application of improved physics-informed neural networks for nonlinear consolidation problems with continuous drainage boundary conditions." Acta Geotechnica **19**(1): 495-508.
- Lan, P., Su, J. and Zhang, S. (2024b). "Surrogate modeling for unsaturated infiltration via the physics and equality-constrained artificial neural networks." Journal of Rock Mechanics and Geotechnical Engineering **16**(6): 2282-2295.
- Lu, L., Pestourie, R., Yao, W., Wang, Z., Verdugo, F. and Johnson, S. G. (2021). "Physics-informed neural networks with hard constraints for inverse design." SIAM Journal on Scientific Computing **43**(6): B1105-B1132.
- Mandl, L., Mielke, A., Seyedpour, S. M. and Ricken, T. (2023). "Affine transformations accelerate the training of physics-informed neural networks of a one-dimensional consolidation problem." Scientific Reports **13**(1): 15566.
- Ni, J., Li, S.-S. and Geng, X.-Y. (2022). "Mechanical and biodeterioration behaviours of a clayey soil strengthened with combined carrageenan and casein." Acta Geotechnica **17**(12): 5411-5427.
- Ouyang, W., Li, G., Chen, L. and Liu, S. W. (2024). "Physics - informed neural networks for large deflection analysis of slender piles incorporating non - differentiable soil - structure interaction." International Journal for Numerical and Analytical Methods in Geomechanics **48**(5): 1278-1308.
- Raissi, M., Perdikaris, P. and Karniadakis, G. E. (2019). "Physics-informed neural networks: A deep learning framework for solving forward and inverse problems involving nonlinear partial differential equations." Journal of Computational physics

378: 686-707.

- Sadiku, S. (2023). "Analysis of Combined Vertical and Radial Consolidation of Soil under Time-Dependent Loading." Civil Engineering Journal.
- Schiassi, E., Furfaro, R., Leake, C., De Florio, M., Johnston, H. and Mortari, D. (2021). "Extreme theory of functional connections: A fast physics-informed neural network method for solving ordinary and partial differential equations." Neurocomputing **457**: 334-356.
- Terzaghi, K. (1943). Theoretical Soil Mechanics.
- Wang, Y., Bai, J., Lin, Z., Wang, Q., Anitescu, C., Sun, J., Eshaghi, M. S., Gu, Y., Feng, X.-Q. and Zhuang, X. (2024a). "Artificial intelligence for partial differential equations in computational mechanics: A review." arXiv preprint arXiv:2410.19843.
- Wang, Y., Shi, C., Shi, J. and Lu, H. (2024b). "Data-driven forward and inverse analysis of two-dimensional soil consolidation using physics-informed neural network." Acta Geotechnica **19**(12): 8051-8069.
- Wu, Z., Zhang, H., Ye, H., Zhang, H., Zheng, Y. and Guo, X. (2024). "PINN enhanced extended multiscale finite element method for fast mechanical analysis of heterogeneous materials." Acta Mechanica **235**(7): 4895-4913.
- Xiang, Z., Peng, W., Liu, X. and Yao, W. (2022). "Self-adaptive loss balanced physics-informed neural networks." Neurocomputing **496**: 11-34.
- Xie, K.-H., Xie, X.-Y. and Jiang, W. (2002). "A study on one-dimensional nonlinear consolidation of double-layered soil." Computers and Geotechnics **29**(2): 151-168.
- Xie, S., Hu, A., Xiao, Z., Mariani, S. and Della Vecchia, G. (2024). "PINN-based approach to the consolidation analysis of visco-elastic soft soil around twin tunnels." Tunnelling and Underground Space Technology **153**: 105981.
- Xu, K., Zhang, N., Yin, Z.-Y. and Li, K. (2025). "Finite element-integrated neural network for inverse analysis of elastic and elastoplastic boundary value problems." Computer Methods in Applied Mechanics and Engineering **436**: 117695.
- Yang, H., Ren, F., Song, Y.-J., Yu, H.-S. and Chen, X. (2025). "Physics-informed neural network solution for thermo-elastic cavity expansion problem." Geomechanics and Geoengineering: 1-11.

- Yang, H., Zhuang, P.-Z., Mo, P.-Q., Yu, H.-S. and Chen, X. (2024). "Analytical solution for transient radial interaction between energy piles and soils: Thermo-elastic cavity expansion analysis." Geomechanics for Energy and the Environment **39**.
- Yin, J.-H. and Graham, J. (1989). "Viscous–elastic–plastic modelling of one-dimensional time-dependent behaviour of clays." Canadian Geotechnical Journal **26**(2): 199-209.
- Yin, J.-H. and Graham, J. (1996). "Elastic visco-plastic modelling of one-dimensional consolidation." Geotechnique **46**(3): 515-527.
- Yuan, B., Heitor, A., Wang, H. and Chen, X. (2024). "Physics-informed Deep Learning to Solve Three-dimensional Terzaghi Consolidation Equation: Forward and Inverse Problems." ArXiv **abs/2401.05439**.
- Zhang, P., Sheil, B., Girolami, M., Yaji, K. and Yin, Z.-Y. (2024a). "A Novel Consolidation Analysis Framework: Universal Function Approximators Regularized by Physical Principles." Canadian Geotechnical Journal(ja).
- Zhang, P., Yin, Z.-Y. and Sheil, B. (2024b). "A physics-informed data-driven approach for consolidation analysis." Géotechnique **74**(7): 620-631.
- Zhou, H., Wu, H., Sheil, B. and Wang, Z. (2025). "A self-adaptive physics-informed neural networks method for large strain consolidation analysis." Computers and Geotechnics **181**: 107131.
- Zhou, J., Zhang, Z., Han, L., Lu, X., Huang, J. and Jin, R. "One-Dimensional Fully Coupled Hydro-Mechanical-Chemical Model for Contaminant Transport Under Step-Loading Condition and Its Analytical Solutions." International Journal for Numerical and Analytical Methods in Geomechanics **n/a**(n/a).